Acta Pharmaceutica Sinica B 2026;16(7):4410−4425

Chinese Pharmaceutical Association
Institute of Materia Medica, Chinese Academy of Medical Sciences

Acta Pharmaceutica Sinica B

www.elsevier.com/locate/apsb
www.sciencedirect.com

SHORT COMMUNICATION

Insights into SARS-CoV-2 replication control *via* targeting the host hijacking function of NSP12

Shirui Fan[a,b], Xinyan Long[c], Wei Zheng[a], Zhengrui Xiang[a,b], Guangjin Liu[d], Miao Luo[d], Yongtang Zheng[c], Ronghua Luo[c], Zezhou Yu[a], Yi Luo[a], Xiaojiang Hao[a,b,*], Duozhi Chen[a,b,*]

[a]*State Key Laboratory of Phytochemistry and Natural Medicines, Kunming Institute of Botany, Chinese Academy of Sciences, Kunming 650201, China*
[b]*Research Unit of Chemical Biology of Natural Anti-Virus Products, Chinese Academy of Medical Sciences, Beijing 100730, China*
[c]*State Key Laboratory of Genetic Evolution & Animal Models, Key Laboratory of Bioactive Peptides of Yunnan Province, KIZ-CUHK Joint Laboratory of Bioresources and Molecular Research in Common Diseases, Kunming Institute of Zoology, Chinese Academy of Sciences, Kunming 650223, China*
[d]*College of Veterinary Medicine, Nanjing Agricultural University, Nanjing 210095, China*

Received 30 July 2025; received in revised form 18 December 2025; accepted 5 January 2026

KEY WORDS

SARS-CoV-2;
NSP12;
Hsc70;
Protein degradation;
Chaperone-mediated autophagy;
Protein accumulation;
Host hijacking function;
Antiviral strategy

Abstract Nonstructural protein 12 (NSP12), the RNA-dependent RNA polymerase (RdRp) of SARS-CoV-2, serves as the catalytic core of the viral replication−transcription complex and is pivotal for viral RNA synthesis. Given its essential role, SARS-CoV-2 must precisely regulate intracellular NSP12 levels to support efficient viral replication. However, the mechanisms governing its stability remain poorly understood. Here, we reveal a previously unrecognized viral strategy in which NSP12 hijacks the host chaperone Hsc70 to modulate its own stability. Mechanistically, Hsc70 plays a dual role: mediating NSP12 degradation *via* chaperone-mediated autophagy (CMA) while also promoting its accumulation. The dynamic balance between these opposing functions determines NSP12 fate. NSP12 can evade CMA-mediated degradation by binding Hsc70 with higher affinity. This disrupts the Hsc70−LAMP2a interaction and shifts Hsc70's role toward primarily facilitating NSP12 accumulation, thereby enhancing viral replication. We identified Hlyc41 as a potential antiviral agent that disrupts this hijacking mechanism. Hlyc41 competes with NSP12 for binding to the F428 residue of Hsc70, thereby promoting NSP12 degradation and suppressing viral replication. These findings reveal a novel host hijacking mechanism that regulates NSP12 levels and support a promising therapeutic strategy targeting this process.

*Corresponding authors.
E-mail addresses: haoxj@mail.kib.ac.cn (Xiaojiang Hao), chenduozhi@mail.kib.ac.cn (Duozhi Chen).

Peer review under the responsibility of Chinese Pharmaceutical Association and Institute of Materia Medica, Chinese Academy of Medical Sciences.

https://doi.org/10.1016/j.apsb.2026.03.055
2211-3835 © 2026 The Authors. Published by Elsevier B.V. on behalf of Chinese Pharmaceutical Association and Institute of Materia Medica, Chinese Academy of Medical Sciences. This is an open access article under the CC BY-NC-ND license (http://creativecommons.org/licenses/by-nc-nd/4.0/).

© 2026 The Authors. Published by Elsevier B.V. on behalf of Chinese Pharmaceutical Association and Institute of Materia Medica, Chinese Academy of Medical Sciences. This is an open access article under the CC BY-NC-ND license (http://creativecommons.org/licenses/by-nc-nd/4.0/).

1. Introduction

The outbreak of the novel coronavirus [severe acute respiratory syndrome coronavirus 2 (SARS-CoV-2)] in 2020 triggered a severe public health crisis in human history, resulting in enormous loss of life and economy. SARS-CoV-2 is a highly contagious, enveloped, single-stranded RNA virus. Its genome encodes four structural proteins, 16 non-structural proteins (NSPs), and several accessory proteins, all of which are critical to the viral life cycle[1,2]. Among these proteins, NSP12 is particularly vital, as it forms the replication−transcription complex (RTC) together with the NSP7 and NSP8 cofactors, which are essential for viral RNA synthesis and gene transcription[2,3]. Structurally, NSP12 comprises a nidovirus RNA-dependent RNA polymerase (RdRp) associated nucleotidyltransferase (NiRAN) domain, an interface domain, and an RdRp domain, with the latter performing the polymerase function[4]. NSP12 has attracted significant attention due to its pivotal role in viral replication[5,6]. However, beyond its well-established catalytic function, research has overlooked that maintaining appropriate intracellular levels of NSP12 is equally critical for the efficient replication of the virus. Thus, as the irreplaceable catalytic component of RTCs, NSP12 levels must be preserved by SARS-CoV-2 to sustain the massive and continuous production of viral RNA during rapid replication.

Autophagy, an evolutionarily conserved mechanism for the degradation of intracellular proteins and organelles, plays a crucial role in maintaining cellular homeostasis and defending against viral infections[7,8]. Based on the mechanism of cargo delivery to lysosomes, autophagy can be broadly classified into three major types: macroautophagy, microautophagy, and chaperone-mediated autophagy (CMA). CMA is a selective lysosomal-degradation pathway specifically targeting proteins bearing KFERQ-like motifs[9]. In this process, the molecular chaperone heat shock cognate 71 kDa protein (Hsc70) recognizes and binds to substrate proteins, directing them to the lysosome. The substrate then interacts with the lysosome-associated membrane protein 2A (LAMP2a) and is unfolded before being translocated into the lysosomal lumen through a multimeric LAMP2a channel for degradation. Upon completion, LAMP2a disassembles into monomers, and Hsc70 is released into the cytosol to initiate a new cycle[10]. This highly selective degradation pathway represents a reliable host antiviral defense strategy by clearing essential viral proteins to suppress viral replication[11,12]. In addition to its role in CMA, Hsc70 performs multiple cellular functions with the assistance of various cochaperones, placing it at a central regulatory node governing protein fate[13-15].

Notably, our study indicates that SARS-CoV-2 NSP12 serves as a potential substrate of the CMA pathway, and Hsc70 is a key host factor in this process. Nonetheless, the robust replication of the virus during infection partially suggests the failure of CMA in degrading NSP12, implying that the virus escapes this clearance through unknown mechanisms. These observations suggest that NSP12 interacts with Hsc70 with substantially more complex functional implications than previously recognized. Investigating this interaction and identifying a chemical probe capable of modulating it to inhibit viral replication represents a meaningful and promising challenge.

2. Materials and methods

2.1. Compounds and reagents

Cycloheximide, Pronase E, Bafilomycin A1, Chloroquine, MG-132, AR7, VER-155008, Geldanamycin, and Remdesivir (MedChemExpress, Shanghai, China) were dissolved in dimethylsulfoxide (DMSO) as stock solutions, followed by storage at −20 °C. The antibodies used were as follows: Hsc70 primary antibody (Abcam, Cambridge, UK); β-actin, GAPDH, SARS-CoV-2 NSP12 primary antibody (Cell Signaling Technology, Danvers, USA); HA, Flag, GFP primary antibody (TransGen Biotech, Beijing, China); Strep and SARS-CoV-2 Nucleocapsid Protein primary antibody, HRP-conjugated mouse anti-DDDDK-Tag, HRP-conjugated goat anti-Mouse, HRP-conjugated goat anti-Rabbit (ABclonal Technology, Wuhan, China); and β-tubulin, LC3B, p62/SQSTM1, ATG5, LAMP2a, HSP90 primary antibody (Abmart, Shanghai, China).

2.2. Cell culture and viruses

HEK293T, Calu-3, and Vero E6 cells were grown in Dulbecco's modified Eagle's medium (Gibco, Grand Island, USA) with 10% fetal bovine serum (Gibco) at 37 °C in a 5% carbon dioxide atmosphere. The prototype SARS-CoV-2 strain was propagated in Vero E6 cells and quantified. Experiments involving this virus were performed at a biosafety level-3 laboratory of Kunming Institute of Zoology, Chinese Academy of Sciences (Kunming, China) or Institute of Medical Biology, Chinese Academy of Medical Sciences (Kunming, China). Unless otherwise specified, experiments were conducted using HEK293T cells.

2.3. Cell infection, treatment, and detection

Cells were seeded in 6- or 12-well plates and incubated for 12 h; the cells were infected with SARS-CoV-2 at a multiplicity of infection of 0.1 for 1 h. After washing twice with phosphate-buffered saline (PBS), the cells were cultured in Dulbecco's modified Eagle's medium supplemented with 2% fetal bovine serum and test compounds for 24 h. The cells were harvested and subjected to western blotting analysis using specific antibodies. Cell supernatants were collected to assess SARS-CoV-2 replication using the 50% tissue culture infectious dose assay, as determined by the Reed−Muench endpoint method. Moreover, RNA was extracted from a portion of the culture supernatant for viral load quantification.

Cells were seeded into 6- or 12-well plates and incubated overnight. After transfection with the indicated plasmids for 24 h, the cells were treated with Hlyc41 or the indicated agents for an

additional 24 h. Unless otherwise specified, Hlyc41 was used at a final concentration of 15 μmol/L.

2.4. Viral load quantification

As previously described[16], RNA was extracted from the cell culture using High Pure Viral RNA Kit (Roche, Basel, Switzerland) according to the manufacturer's instructions, and its concentration was measured. Viral gRNA was quantified *via* real-time qPCR using a one-step RT-qPCR kit (Toyobo, Osaka, Japan) on a ViiA7 Real-Time PCR System (Life Technologies, Carlsbad, USA). The primers for gRNA detection were derived from the nucleocapsid gene of SARS-CoV-2, including forward, 5′-GGGGAACTT CTCCTGCTAGAAT-3′; reverse, 5′-CAGACATTTTGCTCTCAA GCTG-3′; and probe, 5′-FAM-TTGCTGCTGCTTGACAGATT-TAMRA-3′[17].

2.5. Plasmids, transfections, and gene knockdown

Cells were transfected with the indicated plasmids using the jetPRIME reagent (Polyplus, Illkirch, France) according to the manufacturer's instructions. Western blotting was performed to confirm the plasmid expression and siRNA knockdown efficiency. Mutations were generated using the MutExpress II mutagenesis kit (Vazyme, Nanjing, China). Details of the primers used in this study are presented in the Supporting Information Table S1.

The complete coding region of human Hsc70, LAMP2a, HSP90, and HOP was amplified using specific primers *via* PCR employing human cDNA; genes encoding the full-length amino acid sequence of the SARS-CoV-2 spike, membrane, envelope, and nucleocapsid proteins, as well as the NSP5, NSP7, NSP8, and NSP12 proteins were amplified by PCR using specific primers and cDNA from the SARS-CoV-2 isolate Wuhan-Hu-1 (accession No.: NC_045512)[18]. The amplified sequences were then cloned into the indicated vectors, including p3*Flag-CMV-14, pCAGGS-HA, PET28a-His, pCMV-N-mCherry, pEGFP-N1, or pEGFP-C1, to generate plasmids for mammalian expression. The plasmid of Strep-NSP12 (pLVX-EF1alpha-SARS-CoV-2-NSP12-2xStrep-IRES-Puro) was obtained from Miaoling Biosciences (Wuhan, China).

The target siRNA sequences were synthesized by GenePharma (Shanghai, China). Cells were used for subsequent experiments 24 h after siRNA transfection. The siRNA target sequences were as follows: si-Hsc70 (#1, 5′-GGCCAGUAUUGAGAUCGAUTT-3′; #2, 5′-GACCUGCAGUUGGUAUUGATT-3′—unless otherwise specified, #2 was used for Hsc70 knockdown); si-ATG5 (5′-GCAACUCUGGAUGGGAUUGUU-3′); si-LAMP2a (5′-CUG CAAUCUGAUUGAUUAUU-3′); si-HSP90 (#1, 5′-GUAUGACA ACAGCCUCAAGTT-3′; #2, 5′-GGAAAGAGCUGCAUAUUAA TT-3′); and negative control (5′-UUCUCCGAACGUGUCACGU TT-3′).

2.6. KFERQ-like motif analysis

KFERQ-like motifs were identified using the KFERQ finder V0.8 tool (https://rshine.einsteinmed.edu)[19]. This algorithm detects pentapeptide motifs that conform to the canonical KFERQ consensus, defined by the presence of a glutamine (Q) residue flanked by a specific combination of positively charged, negatively charged, and hydrophobic amino acids, as previously described. The full-length amino acid sequences of SARS-CoV-2 nonstructural proteins were retrieved and individually submitted to the "Motifs from sequence" module using default parameters, with standard motifs included in the output. The tool reports all sequence regions that satisfy the predefined KFERQ-like motif criteria.

2.7. Sequence analysis

Sequence conservation of the KFERQ-like motifs in NSP12 among representative β-coronaviruses was assessed using Clustal Omega (https://www.ebi.ac.uk/jdispatcher/msa/clustalo)[20]. The resulting multiple sequence alignment was visualized and annotated using Jalview (https://www.jalview.org)[21].

2.8. Mass spectrometry interactome of NSP12

To further describe the interaction landscape of NSP12 with the host cell proteome, we analyzed the cellular interactome of NSP12 from a previous study conducted by Dr. Muhannad Alruwaili[22]. In that study, high-confidence interactors of both GFP-NSP12 and NSP12-GFP were defined using SAINTexpress with a Bayesian false discovery rate of $\leq$0.05 and an average spectral count of $\geq$2[22]. We used Venny 2.1.0 (https://bioinfogp.cnb.csic.es/tools/venny/index.html) to identify the intersection of high-confidence interactors shared between GFP-NSP12 and NSP12-GFP, and GraphPad Prism was used to plot the Hsc70 protein in the mass spectrometry results.

2.9. Cell viability assay

Cells were seeded in 96-well plates (10,000 cells per well) and incubated for 12 h. The compounds were added in serial concentration and incubated for 48 h. A total of 20 μL of the Enhanced Cell Counting Kit-8 solution (Biosharp, Hefei, China) was added to each well containing 200 μL of cell culture, followed by incubation for another 1 h. Absorbance at 450 nm was measured using a Multiskan™ FC microplate photometer (Thermo Fisher Scientific, Waltham, USA).

2.10. Quantitative real-time polymerase chain reaction

Total RNA was extracted using the RNA-easy Isolation Reagent (Vazyme, Nanjing, China), and its concentration was measured using a NanoDrop 2000 spectrophotometer (Thermo Fisher Scientific). The cDNA was synthesized using the HiScript II 1st Strand cDNA Synthesis Kit (+gDNA wiper) (Vazyme). The mRNA expression levels of target genes were quantified *via* quantitative real-time polymerase chain reaction using ChamQ Universal SYBR qPCR Master Mix (Vazyme) on an Applied Biosystems Real-Time PCR System. Relative mRNA expression levels were calculated using the $2^{-\Delta\Delta CT}$ method. Gene-specific primer sequences (5′−3′) were as follows: β-actin (Forward: CCTGGCACCCAGCACAAT, Reverse: GGGCCGGACTCGTCA TACT), Hsc70 (Forward: TGCTGCTGCTATTGCTTACG, Reverse: TCAATAGTGAGGATTGACACATCA), and NSP12 (Forward: CATGCGAAATGCTGGTATTG, Reverse: TCTGCAGTTAAAGCCCTGGT).

2.11. Western blotting

Cell lysates were boiled in 2 × sodium dodecyl sulfate-polyacrylamide gel electrophoresis (SDS-PAGE) sample loading buffer (Beyotime, Shanghai, China), analyzed *via* SDS-PAGE, and then transferred onto polyvinylidene difluoride membranes

(Millipore, Billerica, USA). The membrane was blocked using 5% nonfat milk powder in tris-buffered saline buffer (Gibco) containing 0.05% Tween 20 for 2 h, followed by incubation with primary antibodies and secondary antibodies. Protein bands were detected using the enhanced electrochemiluminescence chemiluminescent substrate kit (Yeasen, Shanghai, China) and visualized using an enhanced chemiluminescence imager (Tanon, Shanghai, China).

2.12. Immunofluorescence assay

The treated cells were fixed with a 4% polyformaldehyde fixing solution (Beyotime) and then incubated with 4′,6-diamidino-2-phenylindole (Beyotime) for 5 min in the dark. The cells were washed with PBS five times between each step. Finally, the stained cells were examined *via* fluorescence microscopy (Nikon, Tokyo, Japan).

2.13. Co-immunoprecipitation

Cells were washed thrice with cold PBS, followed by lysis with IP lysis buffer (Thermo Fisher Scientific) supplemented with protease inhibitors cocktail (MedChemExpress) on ice for 15 min. The lysates were centrifuged at 12,000 × *g* for 15 min at 4 °C; the supernatants were subsequently transferred to new tubes, followed by incubation with streptavidin agarose beads (MedChemExpress), anti-Flag nanobody agarose beads (AlpalifeBio, Shenzhen, China), or anti-HA nanobody agarose beads (AlpalifeBio) for 2 h or overnight. Alternatively, the supernatants were incubated with the corresponding primary antibodies overnight, followed by incubation with Protein A/G PLUS-Agarose (Santa Cruz Biotechnology, Dallas, TX, USA) for 2 h. After incubation, the beads were washed five times with PBS supplemented with phenylmethylsulfonyl fluoride (Sangon Biotech, Shanghai, China). The immunocomplex was eluted from beads using a 2 × SDS-PAGE sample loading buffer, followed by boiling at 95 °C for 10 min and subsequent immunoblotting analysis.

2.14. Proximity ligation assay (PLA)

PLA was performed using the NaveniFlex Cell Red Kit (Navinci, Uppsala, Sweden) following the manufacturer's instructions with minor modifications[23]. HEK293T cells expressing HA-NSP12 were fixed with 4% paraformaldehyde (Beyotime) for 15 min at room temperature, followed by heat-mediated antigen retrieval in citrate buffer and permeabilized using 0.1% Triton X-100 (Beyotime) for 10 min. After blocking with the supplied buffer, the cells were incubated overnight at 4 °C with LAMP2a and HA primary antibodies, or with LAMP2a primary antibody alone as the negative control. Navenibody conjugates, ligation, and rolling-circle amplification were then applied sequentially following the Navinci protocol. Nuclei were counterstained with DAPI (Beyotime). PLA signals were visualized using the Texas Red channel, and fluorescence images were acquired using a Leica TCS SP8 confocal microscope (Leica Microsystems, Wetzlar, Germany).

2.15. Cell-based SARS-CoV-2 RdRp activity assay

The SARS-CoV-2 polymerase activity assay system used in this study was set up as previously described, with some modifications[24,25]. The plasmid pCoV-Gluc, which produces a positive-strand of vRNA encoding Gluc flanked by SARS-CoV-2 5′ and 3′ UTRs, was purchased from Miaoling Biosciences as the pRetroX-Tight-Puro-Gluc. Briefly, HEK293T cells were transfected with the plasmids CoV-Gluc and HA-NSP12. After 24 h incubation, the cell supernatant was collected and analyzed for Gluc activity using an Infinite 200 PRO microplate reader (TECAN, Männedorf, Switzerland). SARS-CoV-2 RdRp activity was determined based on the relative luciferase signal intensity.

2.16. Cellular thermal shift assay

Transfected HEK293T cells were treated with 50 μmol/L Hlyc41 for 4 h, collected, and resuspended in PBS. Aliquots were heated at the indicated temperatures for 3 min using a T100 thermal cycler (Bio-Rad, Hercules, CA, USA) and then frozen thrice in liquid nitrogen. Soluble proteins were collected *via* centrifugation at 12,000 × *g* for 10 min at 4 °C and subsequently analyzed by immunoblotting.

2.17. Drug affinity-responsive target stability assay

HA-NSP12-transfected HEK293T cells were collected, and the total protein was isolated using IP lysis buffer. The lysate was diluted with TNC buffer (50 mmol/L Tris−HCl at pH 8.0, 50 mmol/L NaCl, and 10 mmol/L $CaCl_2$) and treated with 50 μmol/L Hlyc41 or equal volumes of DMSO. After incubation for 1 h at room temperature, pronase E (25 μg/ml) was added, followed by incubation at 37 °C for 15 min. The reactions were stopped by adding a 2 × SDS-PAGE sample loading buffer, followed by immunoblotting analysis.

2.18. Microscale thermophoresis (MST) analysis

The binding affinities of Hsc70 with LAMP2a, NSP12 with Hsc70, and Hlyc41 with Hsc70 were measured *via* MST analysis. The concentration of recombinant His-tagged Hsc70 proteins was quantified using a bicinchoninic acid protein assay kit (Beyotime). Recombinant LAMP2a (L29-F375) protein was purchased from MCE. For the binding assays, the His-tagged Hsc70 or LAMP2a proteins were labeled using the Monolith His-Tag Labeling Kit RED-tris-NTA 2nd Generation (NanoTemper Technologies, Munich, Germany). Next, Hsc70, NSP12, or Hlyc41 were serially diluted and then incubated with the respective labeled proteins, followed by loading into Monolith standard-treated capillaries. Measurements were performed using a Monolith NT.115 instrument, and the K_d values were determined using the MO. Affinity Analysis software (NanoTemper Technologies).

2.19. Extraction of lysosomes and membrane proteins

Lysosomes were extracted using the lysosome extraction kit (Solarbio, Beijing, China) according to the manufacturer's instructions. Briefly, HEK293T cells were washed with PBS and then lysed in buffer A. After 10 min of incubation, the lysate was manually homogenized using a Teflon homogenizer and centrifuged for 5 min at 1000 × *g*. The resulting supernatant was sequentially centrifuged at 3000 × *g* for 10 min, 5000 × *g* for 10 min, and 20,000 × *g* for 20 min. For lysosome extraction, the insoluble proteins were resuspended in buffer B and centrifuged at 20,000 × *g* for 20 min. The resulting pellet was collected as the membrane protein fraction. Membrane proteins were extracted using the membrane protein extraction kit (Solarbio). Briefly, the insoluble part was collected, resuspended in buffer A *via* shaking

for 30 min, and centrifuged at 12,000 × *g* for 5 min. The resulting supernatant was incubated at 37 °C for 10 min and centrifuged at 1000 × *g* for 5 min (37 °C). The supernatant was collected, and buffer B was added; this mixture was incubated for 2 min on ice and centrifuged at 1000 × *g* for 5 min (37 °C). The resulting supernatant represented the membrane proteins. All procedures were performed at 4 °C unless otherwise specified.

2.20. Statistical analysis

All statistical analyses were performed using GraphPad Prism software, with Student's *t*-test or one-way analysis of variance applied. Data are presented as mean ± standard deviation (SD). $*P < 0.05$, $**P < 0.01$, $***P < 0.001$, $****P < 0.0001$.

3. Results

3.1. SARS-CoV-2 NSP12 degrades via the CMA pathway

CMA substrates possess KFERQ-like motifs that are recognized and bound by Hsc70. To explore the potential susceptibility of SARS-CoV-2 NSPs to CMA-mediated degradation, we first used the KFERQ finder V0.8 tool developed by the Cuervo laboratory[19]. This analysis revealed that multiple SARS-CoV-2 NSPs, including NSP12, harbor one or more KFERQ-like motifs, suggesting that several viral proteins might be subject to CMA regulation (Fig. 1A and Supporting Information Fig. S1A). Considering the essential role of NSP12 in viral RNA synthesis and the limited understanding of NSP12-regulated mechanisms beyond its canonical polymerase activity, we selected NSP12 as the initial focus of our investigation. Subsequent investigations revealed that overexpressed NSP12 interacted with the two central proteins involved in CMA: Hsc70 and LAMP2a (Fig. 1B). The endogenous NSP12 also exhibited the same interaction (Fig. 1C and D). Consistent with this, immunofluorescence staining revealed the co-localization of NSP12 with Hsc70 and LAMP2a (Fig. 1E and Fig. S1B). The PLA also revealed a close spatial association between NSP12 and LAMP2a, supporting the lysosomal localization of NSP12 (Fig. 1F). Moreover, the cell interaction groups of NSP12 reported by Dr. Muhannad Alruwaili[22] indicated the interaction between NSP12 and Hsc70 (Fig. S1C and S1D). These findings suggested that NSP12 can be degraded through the CMA pathway.

Additionally, we also analyzed the binding model of NSP12 to Hsc70. We constructed a series of Hsc70 truncation mutants based on its structural domains (Fig. S1E) and performed binding assays. The results demonstrated that NSP12 specifically interacted with the Hsc70-ΔB1 mutant (Fig. S1F and S1G), indicating that NSP12 engages the substrate-binding domain β (SBDβ) of Hsc70, a key region for substrate recognition, rather than other functional domains. This interaction supported the classification of NSP12 as a CMA substrate. Furthermore, LAMP2a overexpression (the rate-limiting component of CMA) or pharmacological activation of CMA using the specific activator AR7 resulted in a significant CMA-dependent reduction in NSP12 protein levels (Fig. S1H and S1I). Consistent with previous studies, AR7 treatment was associated with enhanced CMA activity, accompanied by increased LAMP2a transcription[26] and protein levels (Fig. S1J). Collectively, these findings provide compelling evidence that NSP12 can be degraded through the CMA pathway.

3.2. Hsc70 promotes the accumulation of NSP12

We discovered that Hsc70 exerted additional regulatory functions on NSP12 besides this role in the CMA pathway. Specifically, the overexpression of Hsc70 markedly increased NSP12 protein levels, as shown *via* immunoblotting analysis and flow cytometry (Fig. 2A and B); however, the knockdown of Hsc70 significantly reduced its expression (Fig. 2C). These findings suggested that Hsc70 plays a positive role in NSP12 production. We further verified whether the increased NSP12 was functionally active through a cell-based assay with Gaussia-luciferase (Gluc) as the reporter to evaluate the SARS-CoV-2 RdRp activity[24]. As expected, NSP12 expression increased the Gluc activity (Fig. 2D). Co-expression of Hsc70 with NSP12 increased both RdRp activity and NSP12 levels, suggesting that the Hsc70-induced increase in NSP12 represents the accumulation of functional NSP12 protein (Fig. 2E).

The ATPase domain of Hsc70, particularly lysine at Position 71, is essential for its folding function[27]. Consistent with this requirement, both treatment with the Hsc70 inhibitor VER-155008, which competitively binds to the ATP-binding pocket[28], and K71A mutant expression of Hsc70 decreased NSP12 levels in a dose-dependent manner (Supporting Information Fig. S2A and S2B). Notably, the reduction induced by the K71A mutation expression was not reversed *via* treatment with Bafilomycin A1 (Fig. S2C), indicating that lysosomal degradation was not involved and implicating impaired accumulation of NSP12 as the primary cause. Hsc70-K71A also lost its ability to promote the accumulation of functional NSP12 (Fig. S2D and S2E). Furthermore, Hsc70 typically functions in cooperation with HSP90 and Hsp70−Hsp90 organizing protein (HOP) during protein quality control in the cells[29,30]. We further confirmed that NSP12 interacted with HSP90 and HOP, indicating that this complex was involved in regulating NSP12 accumulation (Fig. S2F). Thus, the knockdown of HSP90 (Fig. S2G) or its inhibition (Fig. S2H) decreased NSP12 levels, while HSP90 expression increased NSP12 levels (Fig. S2I). Collectively, these findings suggest that Hsc70 promotes the accumulation of functional NSP12, likely functioning in an ATPase-dependent manner and within the chaperone complex (Fig. S2J).

To identify the domains involved in this regulatory function, we co-expressed Hsc70 with four NSP12 truncations (Supporting Information Fig. S3A). The results demonstrated that Hsc70 enhanced NSP12-ΔA and NSP12-ΔB2 levels, indicating its action on the NiRAN and RdRp domains of NSP12 (Fig. S3B and S3C). Binding assays further revealed direct interactions between Hsc70 and the NiRAN, Interface, and RdRp domains of NSP12, corresponding to ΔA, ΔB1, and ΔB2 truncations, respectively (Fig. S3D and S3E). These findings revealed that Hsc70 facilitates the accumulation of NSP12 through a complex, chaperone-mediated mechanism.

3.3. NSP12 hijacks Hsc70 to facilitate viral replication

Building upon the abovementioned findings, we further explored the functional role of Hsc70 in SARS-CoV-2 replication. Although SARS-CoV-2 infection did not alter Hsc70 levels (Fig. 3A), its overexpression increased progeny viral RNA in culture supernatants (Fig. 3B) and nucleocapsid protein (NP) levels (Supporting Information Fig. S4A), suggesting enhanced viral replication. Conversely, Hsc70 knockdown reduced viral

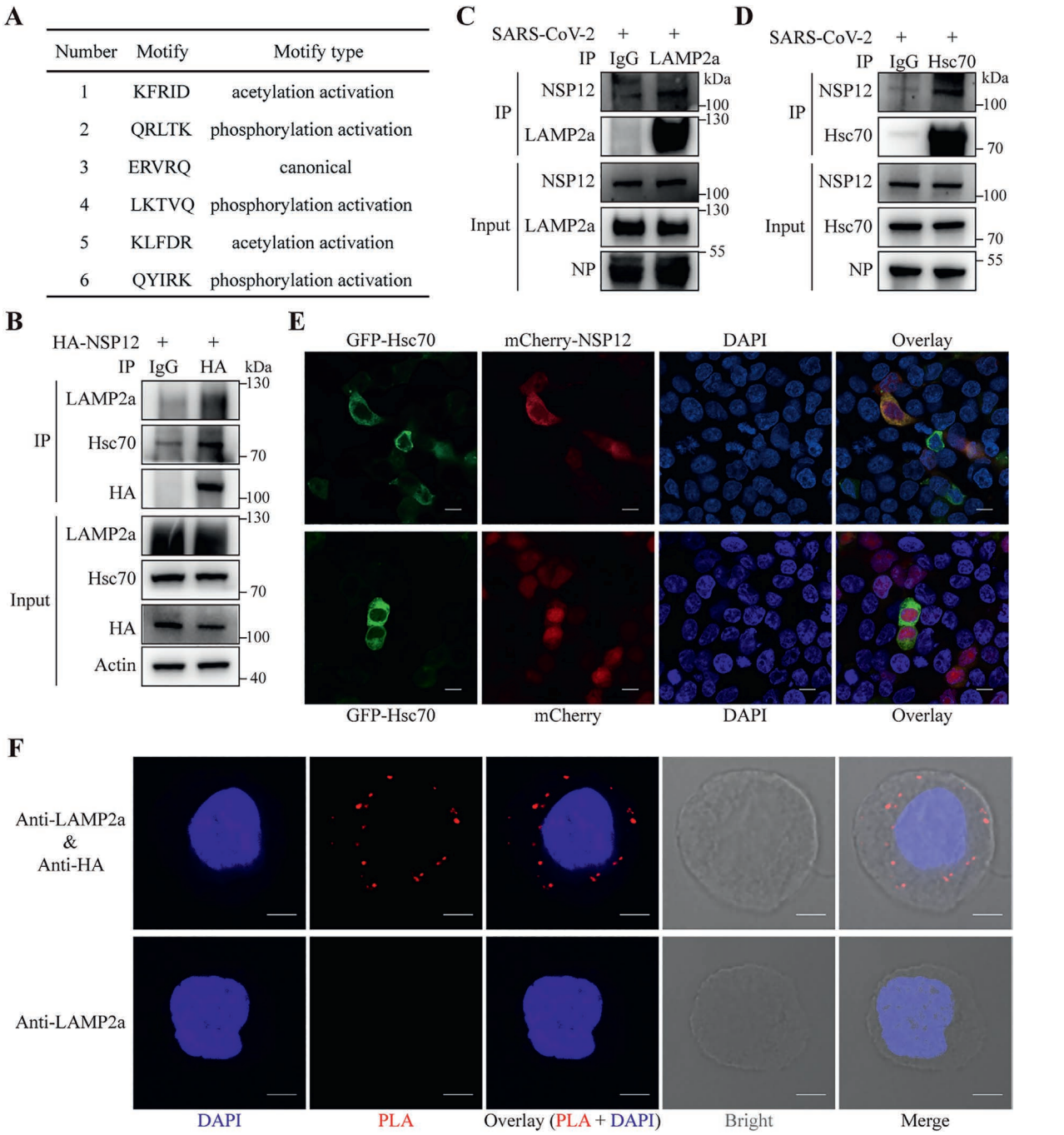

Figure 1 SARS-CoV-2 NSP12 degrades *via* the CMA pathway. (A) The predicted KFERQ-like motifs in NSP12. (B−D) Co-immunoprecipitation assay showing the interaction of NSP12 with Hsc70 and LAMP2a in HEK293T cells (B) and the interaction of endogenous NSP12 with LAMP2a (C) and Hsc70 (D) in SARS-CoV-2 infected Calu-3 cells. (E) Immunofluorescence imaging showing the co-localization of GFP-Hsc70 with mCherry-NSP12 or mCherry. Scale bars = 10 μm. (F) Proximity ligation assay (PLA) showing a close spatial association between HA-NSP12 and LAMP2a. Scale bar = 5 μm.

replication (Fig. 3C and Fig. S4B). These results established Hsc70 as a positive regulator of SARS-CoV-2 replication.

Considering the dual function of Hsc70 on NSP12, we further examined the modulation mechanism of NSP12 levels in SARS-CoV-2 infection. Hsc70 overexpression significantly increased the endogenous abundance of NSP12 (Fig. 3D) and facilitated viral replication, as shown by the 50% tissue culture infectious dose method (Fig. 3E). Meanwhile, the elevation of NSP12 was sufficient to promote viral replication, as shown by NP levels (Fig. 3F) and viral titers (Fig. 3G), as expected. These findings suggested that Hsc70 contributed to viral replication, at least partially, by increasing the NSP12 levels. This function of Hsc70 also suggested that the CMA-dependent degradation of NSP12 occurred at a low rate. Accordingly, we hypothesized that NSP12 might serve as a limiting factor in its own degradation. Supporting this hypothesis, the co-immunoprecipitation assay demonstrated

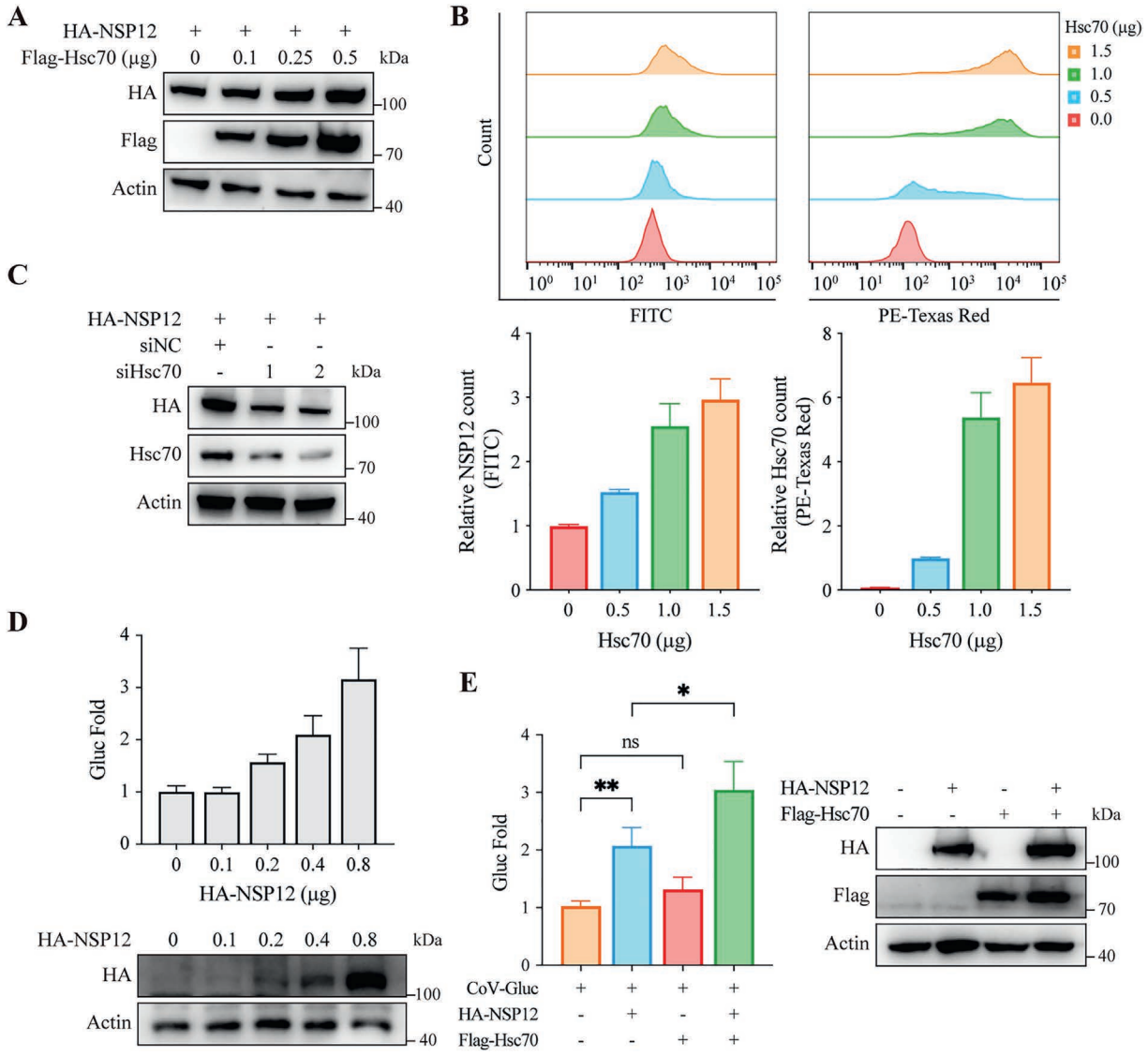

Figure 2 Hsc70 promotes the accumulation of NSP12. (A, B) Hsc70 increases NSP12 protein levels in a dose-dependent manner, as determined *via* immunoblotting analysis (A) and flow cytometry (B). (C) Immunoblotting analysis showing that Hsc70 knockdown reduces NSP12 protein levels. siNC was used as the negative control. (D) Cell-based SARS-CoV-2 RdRp assay showing the NSP12-mediated enhancement of Gluc activity. Data are presented as mean ± SD ($n = 3$). (E) Cell-based SARS-CoV-2 RdRp activity assay showing that the Hsc70-induced accumulation of NSP12 is functionally active. Data are presented as mean ± SD ($n = 3$); ns, not significant, $^*P < 0.05$, and $^{**}P < 0.01$.

that NSP12 disrupted the interaction between Hsc70 and LAMP2a (Fig. 3H). Because the interaction between Hsc70 and LAMP2a ensures the positive occurrence of CMA, this result supports that NSP12 might interfere with its own clearance. The increased concentration of NSP12 interacted with LAMP2a and reduced the binding of Hsc70 to LAMP2a in a dependent manner, demonstrating an inhibitory function (Fig. 3I). Moreover, MST analysis showed that Hsc70 binding to LAMP2a was associated with a dissociation constant (K_d) of 0.51 μmol/L, which shifted to 4.93 μmol/L in the presence of NSP12, indicating that NSP12 interferes with the Hsc70−LAMP2a interaction (Fig. 3J). We preliminarily analyzed the mechanism of the hijacking function of NSP12. MST analysis showed that the binding affinity between Hsc70 and NSP12 was associated with a K_d of 63.84 nmol/L (Fig. 3K). This value is notably higher than that reported for the CMA substrate RNase S peptide, which binds to Hsc70 with a K_d range of 5−8 μmol/L[31-33]. These data indicate that NSP12 binds Hsc70 with relatively high affinity, which might be a method to hijack the Hsc70 function.

Collectively, these findings revealed that NSP12 hijacked Hsc70 to evade CMA-mediated degradation, thereby repurposing Hsc70's function toward promoting NSP12 accumulation. This hijacking mechanism eventually enhances viral replication, highlighting a critical strategy used by SARS-CoV-2 to subvert the host quality control machinery.

3.4. Hlyc41 as a promising lead compound against SARS-CoV-2

Based on the discovery of the hijacking function of NSP12, we hypothesized that small molecules capable of counteracting this hijacking and facilitating NSP12 degradation could serve as antiviral agents. To explore this therapeutic potential, we first

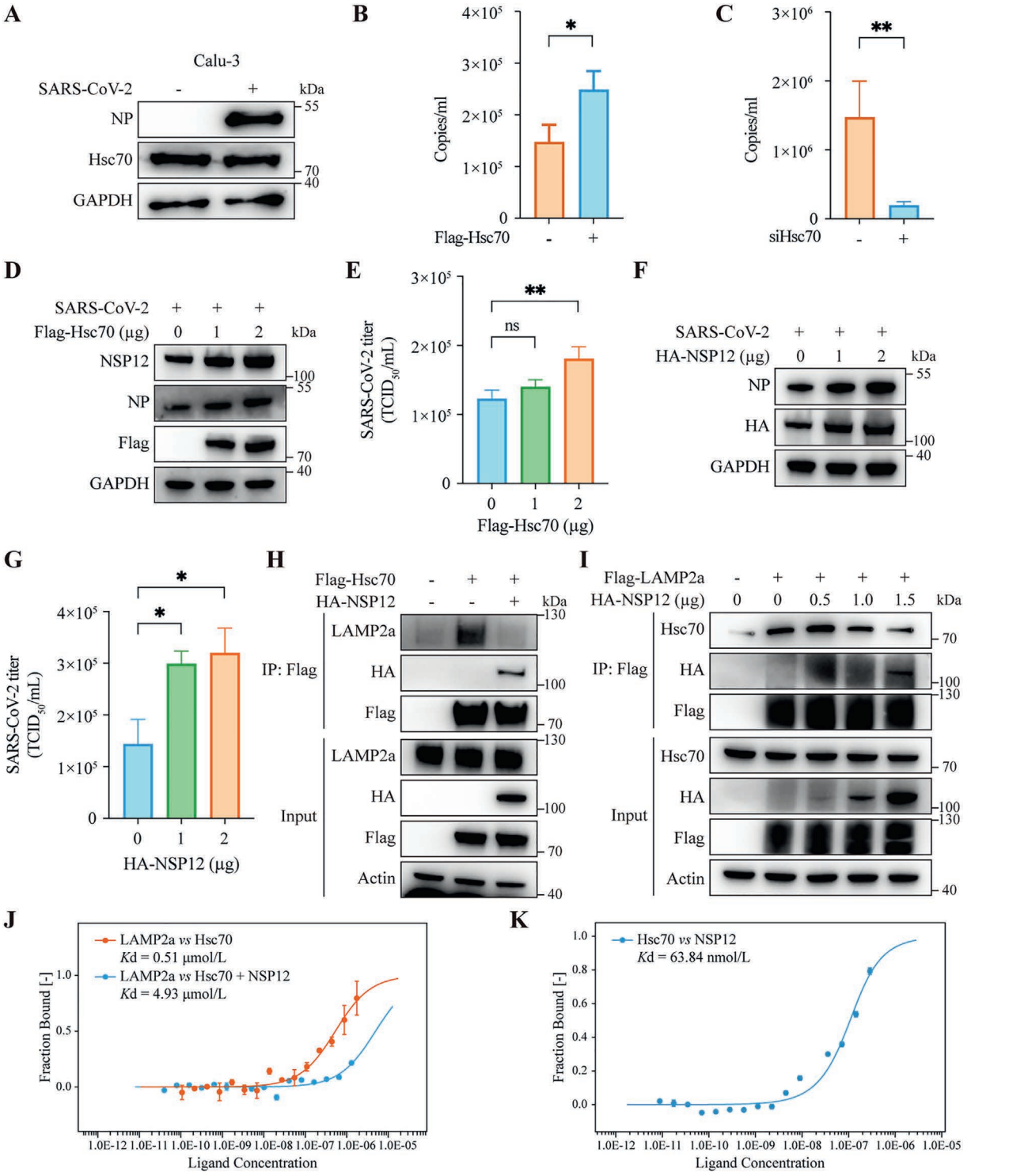

Figure 3 NSP12 hijacks Hsc70 to facilitate SARS-CoV-2 replication. (A) Immunoblot analysis showing that SARS-CoV-2 infection does not alter Hsc70 protein levels. (B, C) Hsc70 facilitates SARS-CoV-2 replication. Viral RNA copies in cell culture with Hsc70 expression (B) or knockdown (C). Data are presented as mean ± SD ($n = 3$); $^{*}P < 0.05$, $^{**}P < 0.01$. (D) Immunoblot analysis showing that Hsc70 increases NSP12 levels in SARS-CoV-2−infected Calu-3 cells. (E) Hsc70 facilitates SARS-CoV-2 replication, as assessed by 50% tissue culture infectious dose ($TCID_{50}$) assay in SARS-CoV-2-infected Calu-3 cells. Data are presented as mean ± SD ($n = 3$); ns, not significant, $^{**}P < 0.01$. (F, G) NSP12 overexpression enhances viral replication in Calu-3 cells, as measured *via* immunoblotting (F) and $TCID_{50}$ assay (G). Data are presented as mean ± SD ($n = 3$); $^{*}P < 0.05$. (H, I) Co-immunoprecipitation assay showing that NSP12 disrupts the interaction between Hsc70 and LAMP2a. (J, K) Microscale thermophoresis analysis showing dissociation constants among the indicated proteins. NSP12 (40 nmol/L) was used in (J). Data are presented as mean ± SD ($n = 3$).

conducted a focused antiviral screen of nearly 200 phenanthridine compounds from our accumulated antiviral compound library, as earlier studies have identified that the phenanthridine compounds exhibit broad-spectrum antiviral activity against hepatitis C, hepatitis B, tobacco mosaic, and porcine epidemic diarrhea viruses[34,35]. This effort identified two structurally related molecules: **Hlyc40** and **Hlyc41** (Fig. 4A). Both molecules exhibited significant antiviral effects *in vitro*. Quantitative analysis of progeny viral RNA in cell cultures revealed that both compounds significantly suppressed viral replication, with half-maximal effective concentrations (EC_{50}) of 2.14 μmol/L for **Hlyc40** and 1.86 μmol/L for **Hlyc41**, indicating their potential as antiviral agents (Fig. 4B). The RdRp inhibitor remdesivir, used as a positive antiviral control in our assay, exhibited an EC_{50} of 2.77 μmol/L,

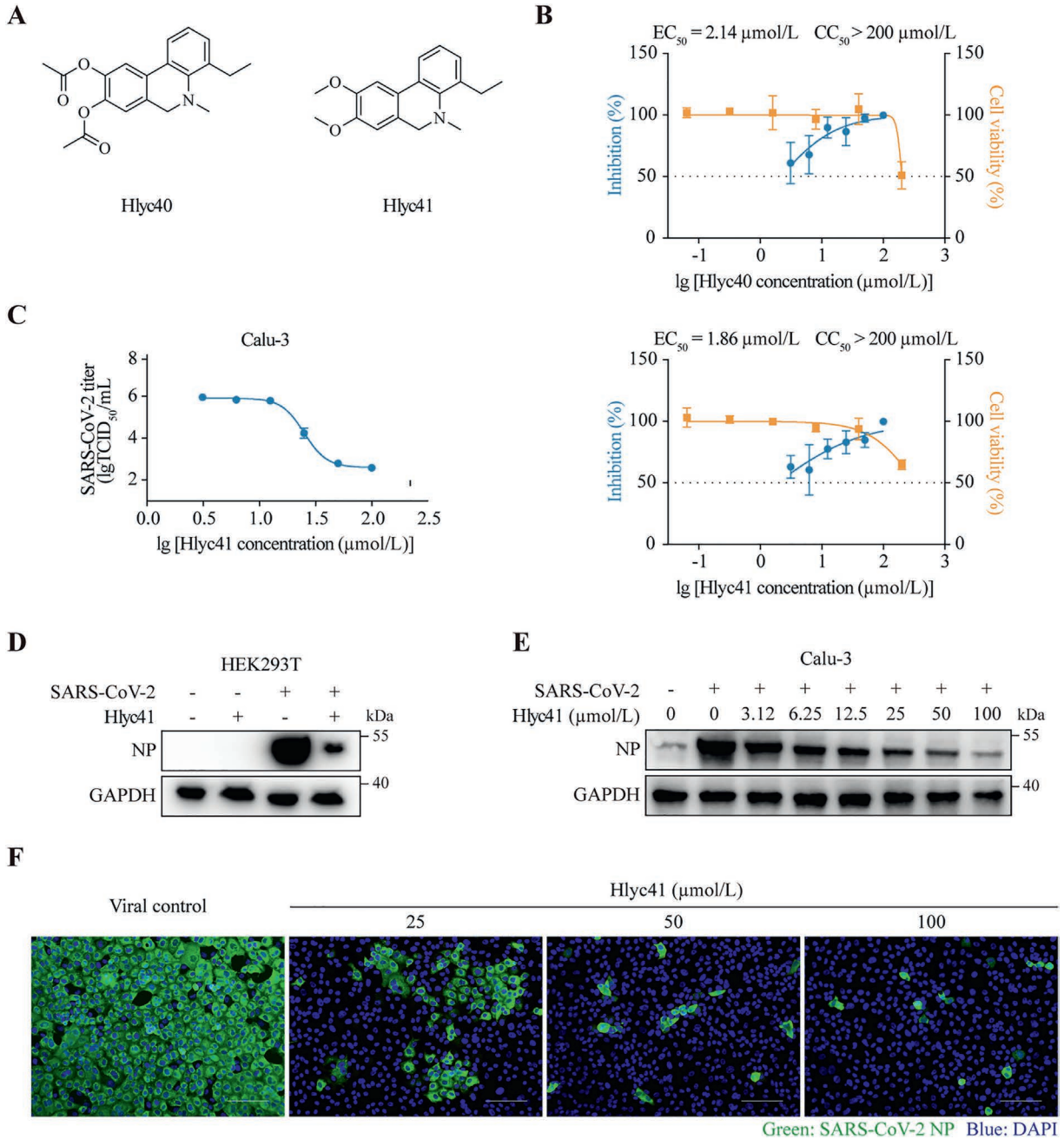

Figure 4 Hlyc41 is a promising lead compound against SARS-CoV-2. (A) Chemical structures of Hlyc40 and Hlyc41. (B) EC_{50} and CC_{50} values of Hlyc40 and Hlyc41. Vero E6 cells were infected with SARS-CoV-2 at a multiplicity of infection of 0.1 and treated with the indicated compounds for 72 h. Extracted viral RNA from the supernatants was used to quantify the viral load, and cell viability was assessed in parallel to calculate the CC_{50}. Data are presented as mean ± SD (n = 3). (C) Hlyc41 reduces viral titers in SARS-CoV-2−infected cell supernatants, as determined using the $TCID_{50}$ assay. Data are presented as mean ± SD (n = 3). (D, E) Immunoblot analysis showing decreased SARS-CoV-2 nucleocapsid protein (NP) expression in SARS-CoV-2-infected cells after treatment with 50 μmol/L (D) or varying concentrations of Hlyc41 (E). (F) Immunofluorescence analysis showing reduced NP signal in SARS-CoV-2−infected Vero E6 cells treated with Hlyc41. Scale bar = 100 μm.

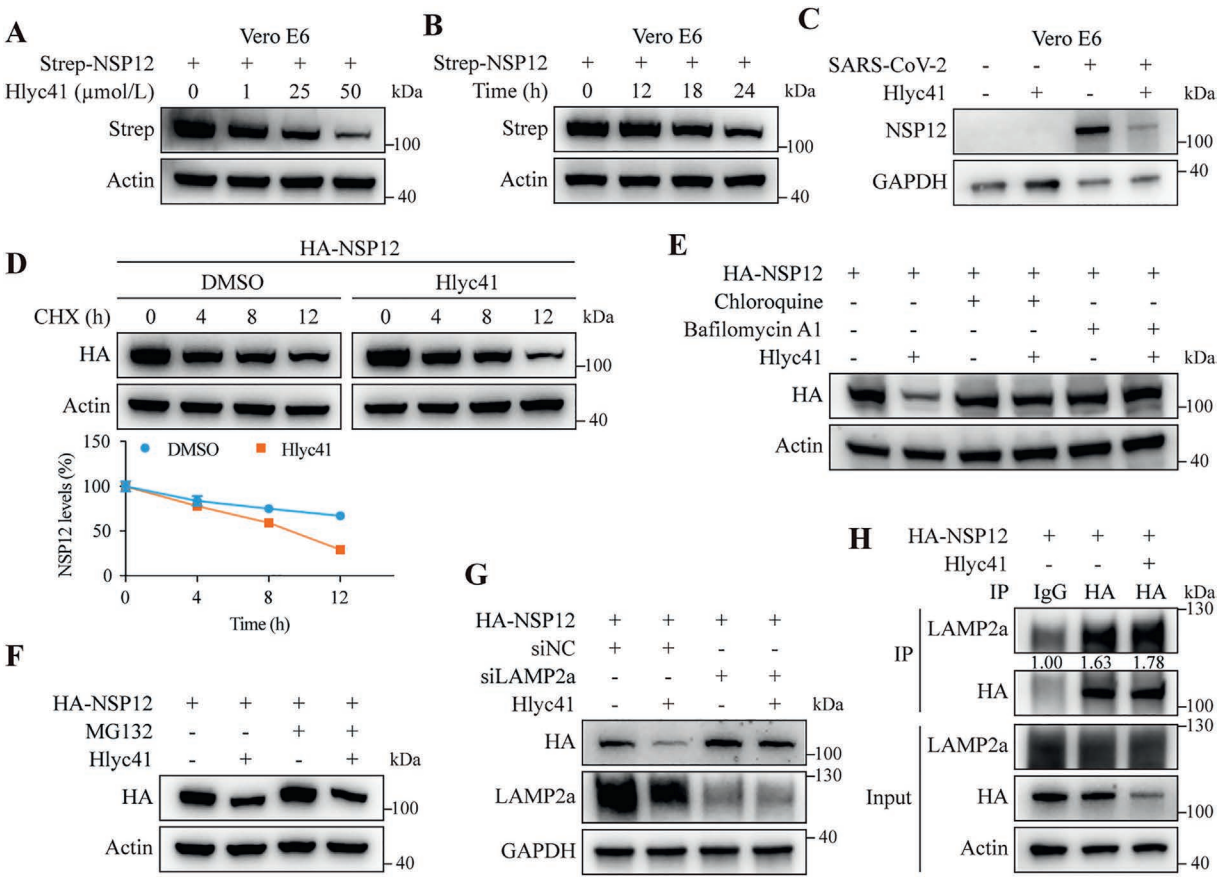

Figure 5 Hlyc41 promotes the CMA-dependent degradation of NSP12. (A, B) Hlyc41 reduces NSP12 levels in a dose- (A) and time- (B) dependent manner, as assessed by immunoblotting. Hlyc41 was used at 25 μmol/L in (B). (C) Endogenous NSP12 levels decrease following Hlyc41 treatment, as shown by immunoblotting. (D) Hlyc41 accelerates NSP12 degradation in the presence of Cycloheximide (CHX, 1 μmol/L), as assessed *via* immunoblotting. (E, F) Lysosomal inhibitors (Chloroquine: 20 mmol/L; Bafilomycin A1: 100 nmol/L), but not the proteasome inhibitor MG132 (10 μmol/L), reverse Hlyc41-induced NSP12 reduction, as shown by immunoblotting. (G) Immunoblotting analysis shows that LAMP2a knockdown abolishes the effect of Hlyc41 on NSP12 degradation. (H) Co-immunoprecipitation assay shows that Hlyc41 enhances the interaction between NSP12 and LAMP2a.

suggesting that the antiviral potencies of **Hlyc40** and **Hlyc41** are comparable to that of a clinically validated polymerase inhibitor (Supporting Information Fig. S5A). Cytotoxicity assessment revealed that the theoretical 50% cytotoxic concentrations (CC_{50}) for both compounds were >200 μmol/L, and the calculated selectivity index (SI=CC_{50} value/EC_{50} value) was >93.46 for **Hlyc40** and > 107.53 for **Hlyc41**, underscoring their therapeutic potentials (Fig. 4B). These findings suggested that phenanthridine derivatives are promising candidates against SARS-CoV-2.

Subsequently, we used various approaches to verify the antiviral efficacy of **Hlyc41**. Viral titer assays demonstrated that **Hlyc41** reduced viral load in a dose-dependent manner, indicating concentration-dependent suppression of viral replication (Fig. 4C). Immunoblotting results showed a dose-dependent reduction in the level of SARS-CoV-2 NP levels following **Hlyc41** treatment, indicating reduced viral content (Fig. 4D and E). Immunofluorescence analysis confirmed a decrease in NP fluorescence intensity, consistent with reduced viral levels (Fig. 4F). **Hlyc41** did not exhibit cytotoxicity at the tested concentrations (Fig. S5B and S5C), further supporting **Hlyc41** as an effective lead antiviral molecule.

3.5. Hlyc41 facilitates the CMA-dependent degradation of NSP12

To analyze the antiviral mechanism of **Hlyc41**, we evaluated its effect on the expression of several key viral proteins (Supporting Information Fig. S6A). Treatment with **Hlyc41** significantly reduced the spike protein and NSP12 levels, while no similar effect was observed with **Hlyc40** (Fig. S6B). Meanwhile, **Hlyc40** was nontoxic at the tested concentration (Fig. S5D). Thus, **Hlyc41** emerged as a lead molecule that exhibited antiviral activity, at least partially, by reducing the NSP12 level, thereby warranting further in-depth research. **Hlyc41** reduced exogenously expressed NSP12 in different cell types in a dose- and time-dependent manner (Fig. 5A and B, Fig. S6C and S6D). In SARS-CoV-2−infected cells, **Hlyc41** also reduced NSP12 levels (Fig. 5C) and induced a dose-dependent decrease in NSP12 and NP levels (Fig. S6E). These results verified that reducing NSP12 protein levels was a main mechanism by which **Hlyc41** suppressed viral replication.

To elucidate the mechanism by which **Hlyc41** reduced NSP12 levels, we first confirmed that it did not affect *NSP12* mRNA

expression, suggesting a post-translational mode of regulation (Supporting Information Fig. S7A). Cycloheximide chase experiments demonstrated that cotreatment with cycloheximide and **Hlyc41** significantly accelerated the decline in NSP12 levels, identifying **Hlyc41** as a potent NSP12 protein degrader (Fig. 5D). Protein degradation mainly occurs *via* the proteasomal or lysosomal pathways. Inhibitor cotreatment experiments showed that lysosomal inhibitors bafilomycin A1 and chloroquine effectively blocked **Hlyc41**-induced NSP12 reduction, confirming lysosome-dependent degradation (Fig. 5E). In contrast, the proteasome inhibitor MG-132 exerted no effect, ruling out proteasomal involvement (Fig. 5F). Considering that NSP12 can be degraded *via* the CMA pathway, we investigated whether **Hlyc41** promoted this process. The knockdown of LAMP2a abolished the **Hlyc41**-induced reduction in NSP12, supporting the involvement of the CMA pathway (Fig. 5G). Although a mild residual reduction in NSP12 levels was still observed, the subsequent experiments yielded no evidence supporting the involvement of other degradation pathways in Hylc41-induced degradation of NSP12. Densitometric analysis of LAMP2a bands pulled down by NSP12 revealed that **Hlyc41** enhanced the interaction, further confirming that **Hlyc41** promoted CMA-mediated degradation of NSP12 (Fig. 5H). We also investigated whether **Hlyc41**-induced degradation occurred *via* macroautophagy. **Hlyc41** did not significantly alter the levels of macroautophagy markers p62 and LC3[36,37], and silencing of ATG5 (required for autophagosome formation)[36,38] did not prevent NSP12 degradation, excluding macroautophagy as a potential pathway (Fig. S7B and S7C). Collectively, these results suggested that **Hlyc41** promotes NSP12 degradation predominantly through a CMA-dependent pathway.

Previous studies reported that Hsc70 downregulation can partially inhibit the replication of other viruses[34,35]. Therefore, we investigated whether **Hlyc41** affected Hsc70 levels. Immunoblotting analysis revealed that **Hlyc41** did not alter Hsc70 levels in either SARS-CoV-2−infected or uninfected cells (Supporting Information Fig. S8A). Although **Hlyc41** reduced NP levels in a dose-dependent manner, Hsc70 levels remained unchanged (Fig. S8B). This finding suggested that **Hlyc41** inhibited SARS-CoV-2 replication and reduced NSP12 levels through a mechanism independent of Hsc70 level modulation.

Using **Hlyc41** as the probe, we further confirmed the functional KFERQ-like motifs of NSP12. Mutating the canonical ERVRQ to ERVAA did not significantly affect **Hlyc41**-induced NSP12 degradation (Supporting Information Fig. S9A). However, simultaneous mutation of all six motifs prevented NSP12 expression, hindering further analysis. Therefore, we shifted our approach to map the positions of the degradation motif by expressing the truncated fragments of NSP12 lacking the NiRAN or RdRp domain (HA-NSP12-ΔA and HA-NSP12-ΔB). **Hlyc41** induced the degradation of both variants (Fig. S9B), and co-immunoprecipitation assays confirmed that both variants interacted with LAMP2a (Fig. S9C). These results suggested that NSP12 has multiple functional KFERQ-like motifs distributed across both domains. Subsequent individual mutations of LKTVQ to LKTAA and QYIRK to AAIRK blocked the degradation of variants, confirming them as functional KFERQ-like motifs of NSP12 (Fig. S9D−S9F). Furthermore, we examined the solvent accessibility and evolutionary conservation of these two KFERQ-like motifs in NSP12. Structural analysis showed that both motifs were exposed on the protein surface, suggesting their potential accessibility (Fig. S9G). Conservation analysis further showed that the motif within the RdRp domain (QYIRK) is relatively well preserved across representative β-coronaviruses (Fig. S9H), implying that the NSP12 degradation mechanism might be conserved in multiple β-coronaviruses. These findings further established NSP12 as a CMA substrate.

3.6. Hlyc41 inhibits viral replication by directly targeting the host protein Hsc70

Hlyc41 does not increase LAMP2a levels or degrade the endogenous CMA substrate GAPDH[39] or the exogenous CMA substrate MEF2D[40], indicating that it does not broadly activate CMA but specifically facilitates NSP12 degradation *via* this pathway (Supporting Information Fig. S10A−S10C). Moreover, **Hlyc41** does not affect the Hsc70−HSP90 and HOP−HSP90 interactions (Fig. S10D and S10E) or Hsc70 ATPase activity even at high concentrations (Fig. S10F), indicating that **Hlyc41** does not interfere with the function of Hsc70 in promoting the accumulation of NSP12. Collectively, these results suggested that **Hlyc41** might exert its effect by directly targeting the Hsc70 protein.

Therefore, we used a reported biotinylated **Hlyc41** probe **HLY179** for target hooking[41]. Treatment with **HLY179** reduced NSP12 levels, consistent with the activity of **Hlyc41**, albeit with slightly diminished potency likely owing to the biotin modification (Supporting Information Fig. S11). **HLY179** effectively captured endogenous and recombinant Hsc70 proteins, indicating specific binding between **HLY179** and **Hsc70** (Fig. 6A and B). Moreover, excess **Hlyc41** competitively inhibited the interaction between **HLY179** and the recombinant Hsc70, suggesting a shared binding mode between **HLY179** and **Hlyc41** (Fig. 6B). These observations were further validated *via* label-free target identification techniques. A cellular thermal shift assay showed increased thermal stability of Hsc70 upon **Hlyc41** treatment, indicating a ligand-dependent stabilizing interaction (Fig. 6C). Similarly, drug affinity-responsive target stability analysis supported this direct interaction (Fig. 6D). Moreover, MST analysis revealed a strong binding affinity between **Hlyc41** and Hsc70, with a K_d of 41.31 nmol/L, which is substantially close to those of NPS12 and Hsc70 (Fig. 6E). Furthermore, structural modeling of the human Hsc70-SBD using AlphaFold yielded two distinct conformations: (i) Model 1 featured an open α-helical lid, and (ii) Model 2 showed that the lid folds over the SBDβ subdomain (Supporting Information Fig. S12). Given that Hsc70 usually forms a closed conformation after binding to the substrate protein, Model 2 was selected for subsequent molecular-docking analysis. Using AutoDock Vina, **Hlyc41** was predicted to bind the SBDβ subdomain of Hsc70 with a binding affinity of −7.1 kcal/mol (Fig. 6F). Collectively, these results confirmed that **Hlyc41** directly targets Hsc70. Further functional validation of Hsc70 revealed its essential role in the antiviral mechanism of **Hlyc41**. Knockdown of Hsc70 significantly impaired **Hlyc41**-mediated degradation of NSP12 and reduced its antiviral effect in cell supernatants (Fig. 6G and H). Conversely, overexpression of Hsc70 enhanced the **Hlyc41**-induced reduction in viral titers (Fig. 6I). These findings firmly established Hsc70 as the direct and functional target of **Hlyc41**.

3.7. Hlyc41 antagonizes the hijacking function of NSP12 by competing with it for the F428 site of Hsc70

We performed co-immunoprecipitation assays to further elucidate the molecular mechanism and critical binding interface of **Hlyc41**. The results revealed that HLY179 bound to Hsc70-ΔB1,

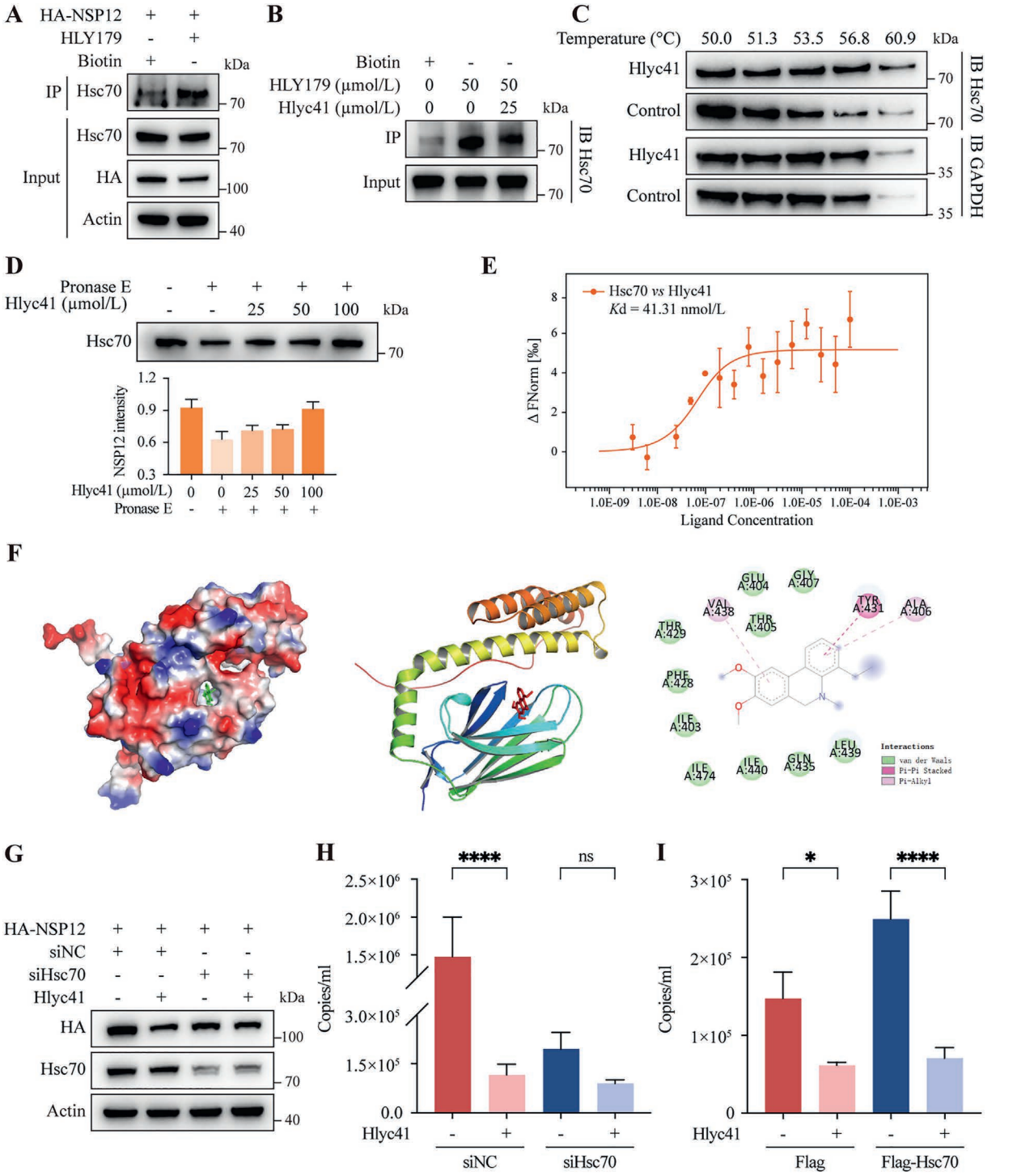

Figure 6 Hlyc41 inhibits viral replication by directly targeting the host protein Hsc70. (A) Co-immunoprecipitation assay showing the interaction between HLY179 and Hsc70 in transfected HEK293T cells treated with 100 μmol/L of HLY179 or biotin for 12 h. (B) Co-immunoprecipitation assay showing the interaction between HLY179 and recombinant Hsc70 *in vitro*; recombinant Hsc70 protein was incubated with the indicated molecules for 2 h. (C) Cellular thermal shift assay and (D) drug affinity-responsive target stability assay confirming Hlyc41−Hsc70 binding; GAPDH serves as a negative control (D). (E) Microscale thermophoresis analysis demonstrating direct binding between Hlyc41 and Hsc70. Data are presented as mean ± SD ($n = 3$). (F) Molecular-docking analysis of Hlyc41 binding to Hsc70-SBD (Model 2). (G) Hsc70 knockdown impairs Hlyc41-mediated NSP12 reduction, as shown *via* immunoblotting. (H, I) Hsc70 knockdown (H) or overexpression (I) modulates the antiviral activity of Hlyc41. Data are presented as mean ± SD ($n = 3$); ns, not significant, $^*P < 0.05$, and $^{****}P < 0.0001$.

indicating that **Hlyc41** interacted specifically with the SBDβ domain of Hsc70 (Fig. 7A and B). Molecular docking using AutoDock Vina showed that **Hlyc41** fitted into the hydrophobic, substrate-binding pocket of SBD, identifying four potential interacting residues (Fig. 7C). Site-directed mutagenesis of these residues to valine (V) or alanine (A), followed by co-immunoprecipitation, showed that the mutation of phenylalanine at position 428 (F428) nearly abolished the interaction between HLY179 and Hsc70 (Fig. 7D and Supporting Information Fig. S13). Notably, this mutation also impaired the ability of **Hlyc41** to facilitate NSP12 degradation (Fig. 7E), confirming that F428 in Hsc70 is a key binding site for **Hlyc41**. We also examined an alternative interaction mode predicted *via* Model 1. AutoDock Vina docking suggested a binding affinity of −5.9 kcal/mol (Supporting Information Fig. S14A). **Hlyc41** interacted with the lid region of SBD and involved two putative binding residues

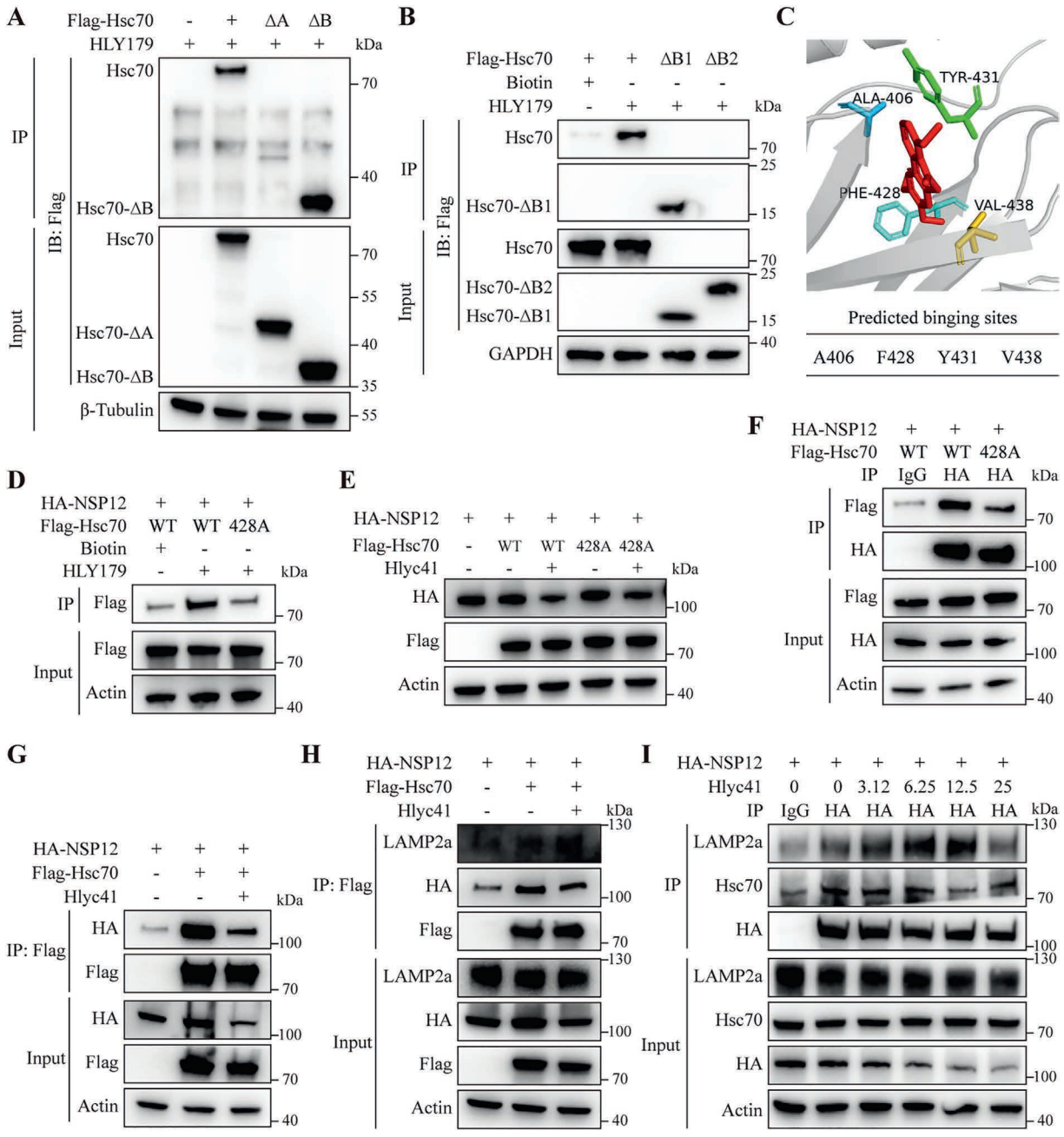

Figure 7 Hlyc41 antagonizes the hijacking function of NSP12 by competing with it for the F428 site of Hsc70. (A, B) Co-immunoprecipitation assay showing that HLY179 binds to the SBDβ domain of Hsc70. (C) Molecular-docking analysis showing the predicted binding mode of Hlyc41 based on Model 2. (D) Co-immunoprecipitation assay showing the reduced Hsc70-428A mutant binding to HLY179. (E) Immunoblotting analysis showing that the 428A mutation of Hsc70 blocks Hlyc41-induced NSP12 degradation. (F) Co-immunoprecipitation showing weakened NSP12 binding to Hsc70-F428A. (G, H) Co-immunoprecipitation assay showing that Hlyc41 reduces Hsc70−NSP12 interaction (G) and induces Hsc70−LAMP2a interaction (H). (I) Co-immunoprecipitation assay showing that Hlyc41 induces NSP12−LAMP2a interaction and reduces NSP12−Hsc70 interaction.

(Fig. S14B). As expected, mutating these residues did not affect the interaction between HLY179 and Hsc70 (Fig. S14C), effectively excluding this binding mode.

We next assessed the influence of mutations at the proposed **Hlyc41**-binding residues on the Hsc70−NSP12 interaction. The F428 mutation also markedly disrupted the binding of Hsc70 to NSP12, whereas other site mutations exerted no such effect (Fig. 7F and Supporting Information Fig. S15), suggesting that **Hlyc41** and NSP12 competitively bound to the F428 site of Hsc70. This competitive mechanism was further supported by co-immunoprecipitation assays, demonstrating that **Hlyc41** reduced the interaction between Hsc70 and NSP12 in intact cells (Fig. 7G) and in cell lysates (Supporting Information Fig. S16).

Subsequently, we analyzed the downstream functions of **Hlyc41**. **Hlyc41** promoted the interaction between Hsc70 and LAMP2a by inhibiting the binding of NSP12 to Hsc70, effectively suppressing the hijacking effect of NSP12 (Fig. 7H). This effect was dose-dependent and enhanced the association between NSP12 and LAMP2a, eventually accelerating NSP12 degradation (Fig. 7I). To investigate downstream lysosomal events, we treated isolated lysosomes with **Hlyc41** and examined the lysosomal membrane fraction. **Hlyc41** promoted the dissociation of Hsc70 from the lysosomal membrane (Supporting Information Fig. S17), indicating that the compound facilitated Hsc70 release independent of the cytosolic factor—a downstream effect consistent with CMA activation.

4. Discussion

Although the global threat posed by SARS-CoV-2 has diminished, understanding its molecular biology and developing host-targeting antiviral strategies remain essential for future preparedness. Viral NSPs are central to replication and represent attractive therapeutic targets[25,42,43]. As research progresses, increasing attention has been directed toward the homeostasis of these key NSPs and their significance in viral replication[44]. Given that NSP12 constitutes the catalytic core of RTCs, elucidating its mechanisms of escape from CMA-mediated degradation and using small molecules to inhibit this evasion while facilitating targeted degradation is of considerable significance. In this study, we systematically characterized the host-mediated regulation of NSP12 and identified an antiviral agent capable of modulating its degradation.

Our study identifies Hsc70 as a key host regulator of NSP12. Hsc70 exerts a dual function on NSP12, both promoting its accumulation and targeting it for degradation *via* the CMA pathway. The balance between these opposing activities determines the level of NSP12 and, consequently, influences viral replication. Future studies could examine how this balance is dynamically regulated in infected cells and how viral or host factors shift Hsc70 activity toward promoting accumulation or degradation, potentially providing new insights into viral replication.

Although folding and degradation are typical functions of Hsc70, its extent of interaction with NSP12 was unexpected. Hsp70-family proteins typically recognize short, abundant hydrophobic motifs, which explains the broad interaction pattern observed throughout NSP12 and the role of Hsc70 in promoting the accumulation of multiple subdomains of NSP12[45-47]. In contrast, CMA requires specific recognition of KFERQ-like motifs, indicating that Hsc70 uses distinct recognition mechanisms to regulate the accumulation versus degradation of NSP12. These findings highlight mechanistic diversity in Hsc70 regulation that warrants further investigation.

Maintaining the homeostasis of viral proteins is crucial for viral replication[48]. In this study, we determined that NSP12 exploited the dual function of Hsc70 to escape CMA-mediated degradation, revealing an additional host factor hijacking strategy. While the formation of double-membrane vesicles (DMVs) protects RTC components from host degradation mechanisms, DMVs are absent during the earliest phase of infection[49]. NSP12, translated from incoming viral genomic RNA, initially localizes in the cytosol, where it is most likely exposed to CMA. Accordingly, our results suggest that NSP12 escapes CMA-mediated degradation by hijacking Hsc70, which might function to ensure its accumulation before the formation of and localization to DMVs. Thus, this mechanism likely operates during the early stage of infection and warrants further investigation. This study also underscores that several NSPs likely possess underappreciated functions throughout infection, and their systematic characterization might reveal new antiviral targets.

Notably, promoting the degradation of viral proteins to counteract mutation-induced resistance has emerged as an effective antiviral strategy[50,51]. In this study, we showed that enhancing the CMA-dependent degradation of NSP12 markedly suppressed viral replication. Given that the KFERQ-like motif (QYIRK) in NSP12 appears to be conserved across some β-coronaviruses and that additional KFERQ-like motifs are also present in other NSPs, we suggest that CMA might broadly function across related viruses. Further exploration of this pathway and the development of targeted interventions might provide valuable adjuvant therapeutic strategies.

We identified a phenanthridine derivative, **Hlyc41**, that disrupts NSP12-mediated hijacking by competitively binding Hsc70 at the NSP12-interacting site. This restores the Hsc70−LAMP2a association and promotes NSP12 degradation. Considering the role of Hsc70 in delivering cytosolic substrates (in this case, NSP12) to the lysosome, a key question arises: if competitive binding occurs in the cytosol, how is lysosomal targeting of NSP12 achieved? Our results show that NSP12 and **Hlyc41** have comparable binding affinities for Hsc70, indicating a dynamic equilibrium during competition. Furthermore, similar to the iterative binding of Hsc70 during protein folding[52], the two KFERQ-like motifs in NSP12 might allow sequential binding to Hsc70. When the interaction of one motif with Hsc70 is blocked by **Hlyc41**, the released NSP12 could rapidly rebind to a nearby Hsc70 *via* the second motif, facilitating lysosomal targeting. Finally, conformational changes in NSP12 upon binding to LAMP2a at the lysosomal membrane might shift the competitive balance, enabling CMA to proceed. Given the complexity of this mechanism, further clarification of the lysosomal targeting mechanism of substrate proteins represents a promising direction in CMA pathway research.

Hlyc41 represents an attractive host-targeting antiviral lead compound. Although the mechanism of **Hlyc41** differs from that of nucleotide analog inhibitors, which directly target RdRp (*e.g.*, remdesivir, GS-441524, and molnupiravir), its EC_{50} (1.86 μmol/L) is within a comparable potency range[53]. Given the complexity of cellular mechanisms, small molecules might cause unpredictable interactions and outcomes within cells. Therefore, specific targeting of host functions becomes particularly important. This study shows that **Hlyc41** promotes NSP12 degradation *via* the CMA pathway by targeting Hsc70, without broadly activating the pathway. Further in-depth studies are required to explore the

bioactivity of the binding site of **Hlyc41** and investigate its role in regulating Hsc70 function. Alternatively, from a structural perspective, further research into the interaction mechanisms between NSP12 and Hsc70 would help clarify how **Hlyc41** achieves specificity. Additionally, artificial intelligence-assisted drug design methods could be used to optimize the antiviral activity of lead compounds by studying the binding patterns of small molecules to binding sites. This study focused on discovering and elucidating host−virus interactions, advancing the understanding of viral physiology, and providing new strategies for developing small-molecule drugs targeting the host.

Our results elucidate the reciprocal interplay between Hsc70 and NSP12, including how NSP12 hijacks Hsc70 and how **Hlyc41** rescues Hsc70 to regulate NSP12 levels, ultimately affecting viral replication. These findings highlight CMA as a critical node in the host antiviral defense and a potential intervention target against viral infection. Moreover, this study indicates Hsc70 as a promising target for anti-SARS-CoV-2 drug development, offering new avenues for future antiviral drug discovery.

5. Conclusions

In this study, we identified the host protein Hsc70 as a key interaction partner of NSP12. Hsc70 exerted a dual function on NSP12: facilitating the accumulation of NSP12 and targeting it for CMA-dependent degradation. Remarkably, NSP12 hijacks this system by leveraging its high affinity for Hsc70 to disrupt Hsc70−LAMP2a interaction, thereby evading CMA-dependent degradation. Building on this mechanism, we developed the targeted antiviral lead compound **Hlyc41**, which competes with NSP12 for Hsc70 binding with comparable affinity, restores Hsc70−LAMP2a and NSP12−LAMP2a interactions, thereby promoting CMA-dependent NSP12 degradation. This study provides new insights into SARS-CoV-2 NSP12 regulation and proposes a targeted small-molecule regulatory strategy.

Acknowledgments

Strategic Priority Research Program of the Chinese Academy of Sciences (XDB1230303, China), CAMS Innovation Fund for Medical Sciences (2021-I2M-5-004, China), Key Research and Development Project of Yunnan Province (202203AC100009, China), National Natural Science Foundation of China (82293683, China), and Open Research Fund of Yunnan Characteristic Plant Extraction Laboratory (2022YKZY001, YKKF2024005, China).

Author contributions

Supervision: Xiaojiang Hao, Duozhi Chen. Conceptualization: Xiaojiang Hao, Duozhi Chen, Shirui Fan, Yongtang Zheng, and Ronghua Luo. Methodology and investigation: Shirui Fan, Xinyan Long, Wei Zheng, Guangjin Liu, Miao Luo, Zhengrui Xiang, Zezhou Yu, and Yi Luo. Writing - original draft: Shirui Fan. Writing - review & editing: Xiaojiang Hao, Duozhi Chen, and Shirui Fan. All the authors have read and approved the final manuscript.

Conflicts of interest

The authors declare no conflicts of interest.

Appendix A. Supporting information

Supporting information to this article can be found online at https://doi.org/10.1016/j.apsb.2026.03.055.

References

1. Lu R, Zhao X, Li J, Niu P, Yang B, Wu H, et al. Genomic characterisation and epidemiology of 2019 novel coronavirus: implications for virus origins and receptor binding. *Lancet* 2020;**395**:565−74.
2. Brant AC, Tian W, Majerciak V, Yang W, Zheng ZM. SARS-CoV-2: from its discovery to genome structure, transcription, and replication. *Cell Biosci* 2021;**11**:136.
3. Hillen HS, Kokic G, Farnung L, Dienemann C, Tegunov D, Cramer P. Structure of replicating SARS-CoV-2 polymerase. *Nature* 2020;**584**:154−6.
4. Gao Y, Yan L, Huang Y, Liu F, Zhao Y, Cao L, et al. Structure of the RNA-dependent RNA polymerase from COVID-19 virus. *Science* 2020;**368**:779−82.
5. Maio N, Lafont BAP, Sil D, Li Y, Bollinger Jr JM, Krebs C, et al. Fe−S cofactors in the SARS-CoV-2 RNA-dependent RNA polymerase are potential antiviral targets. *Science* 2021;**373**:236−41.
6. Xu T, Li K, Huang S, Ivanov KI, Yang S, Ji Y, et al. Anti-SARS-CoV-2 prodrug ATV006 has broad-spectrum antiviral activity against human and animal coronaviruses. *Acta Pharm Sin B* 2025;**15**:2498−510.
7. Mizushima N, Komatsu M. Autophagy: renovation of cells and tissues. *Cell* 2011;**147**:728−41.
8. Deretic V, Saitoh T, Akira S. Autophagy in infection, inflammation and immunity. *Nat Rev Immunol* 2013;**13**:722−37.
9. Dice JF, Chiang HL, Spencer EP, Backer JM. Regulation of catabolism of microinjected ribonuclease A. Identification of residues 7-11 as the essential pentapeptide. *J Biol Chem* 1986;**261**:6853−9.
10. Kaushik S, Cuervo AM. The coming of age of chaperone-mediated autophagy. *Nat Rev Mol Cell Biol* 2018;**19**:365−81.
11. Orvedahl A, MacPherson S, Sumpter Jr R, Talloczy Z, Zou Z, Levine B. Autophagy protects against Sindbis virus infection of the central nervous system. *Cell Host Microbe* 2010;**7**:115−27.
12. Sumpter Jr R, Levine B. Selective autophagy and viruses. *Autophagy* 2011;**7**:260−5.
13. Liu T, Daniels CK, Cao S. Comprehensive review on the HSC70 functions, interactions with related molecules and involvement in clinical diseases and therapeutic potential. *Pharmacol Ther* 2012;**136**:354−74.
14. Bukau B, Weissman J, Horwich A. Molecular chaperones and protein quality control. *Cell* 2006;**125**:443−51.
15. Gu X, Zheng M, Gao Y, Lin S, Zhang X, Chen C, et al. Overview of host-directed antiviral targets for future research and drug development. *Acta Pharm Sin B* 2025;**15**:1723−51.
16. Pang W, Lu Y, Zhao YB, Shen F, Fan CF, Wang Q, et al. A variant-proof SARS-CoV-2 vaccine targeting HR1 domain in S2 subunit of spike protein. *Cell Res* 2022;**32**:1068−85.
17. Qiao J, Li YS, Zeng R, Liu FL, Luo RH, Huang C, et al. SARS-CoV-2 M^{pro} inhibitors with antiviral activity in a transgenic mouse model. *Science* 2021;**371**:1374−8.
18. Wu F, Zhao S, Yu B, Chen YM, Wang W, Song ZG, et al. A new coronavirus associated with human respiratory disease in China. *Nature* 2020;**579**:265−9.
19. Kirchner P, Bourdenx M, Madrigal-Matute J, Tiano S, Diaz A, Bartholdy BA, et al. Proteome-wide analysis of chaperone-mediated autophagy targeting motifs. *PLoS Biol* 2019;**17**:e3000301.
20. Madeira F, Pearce M, Tivey ARN, Basutkar P, Lee J, Edbali O, et al. Search and sequence analysis tools services from EMBL-EBI in 2022. *Nucleic Acids Res* 2022;**50**:W276−9.
21. Waterhouse AM, Procter JB, Martin DM, Clamp M, Barton GJ. Jalview version 2—a multiple sequence alignment editor and analysis workbench. *Bioinformatics* 2009;**25**:1189−91.

22. Alruwaili M, Armstrong S, Prince T, Erdmann M, Matthews DA, Luu L, et al. SARS-CoV-2 NSP12 associates with TRiC and the P323L substitution acts as a host adaption. *J Virol* 2023;**97**:e0042423.
23. Soderberg O, Gullberg M, Jarvius M, Ridderstrale K, Leuchowius KJ, Jarvius J, et al. Direct observation of individual endogenous protein complexes *in situ* by proximity ligation. *Nat Methods* 2006;**3**: 995−1000.
24. Zhao J, Guo S, Yi D, Li Q, Ma L, Zhang Y, et al. A cell-based assay to discover inhibitors of SARS-CoV-2 RNA dependent RNA polymerase. *Antivir Res* 2021;**190**:105078.
25. Li Q, Yi D, Lei X, Zhao J, Zhang Y, Cui X, et al. Corilagin inhibits SARS-CoV-2 replication by targeting viral RNA-dependent RNA polymerase. *Acta Pharm Sin B* 2021;**11**:1555−67.
26. Anguiano J, Garner TP, Mahalingam M, Das BC, Gavathiotis E, Cuervo AM. Chemical modulation of chaperone-mediated autophagy by retinoic acid derivatives. *Nat Chem Biol* 2013;**9**:374−82.
27. O'Brien MC, Flaherty KM, McKay DB. Lysine 71 of the chaperone protein Hsc70 is essential for ATP hydrolysis. *J Biol Chem* 1996;**271**: 15874−8.
28. Williamson DS, Borgognoni J, Clay A, Daniels Z, Dokurno P, Drysdale MJ, et al. Novel adenosine-derived inhibitors of 70 kDa heat shock protein, discovered through structure-based design. *J Med Chem* 2009;**52**:1510−3.
29. Moran Luengo T, Mayer MP, Rudiger SGD. The Hsp70−Hsp90 chaperone cascade in protein folding. *Trends Cell Biol* 2019;**29**:164−77.
30. Johnson BD, Schumacher RJ, Ross ED, Toft DO. Hop modulates Hsp70/Hsp90 interactions in protein folding. *J Biol Chem* 1998;**273**: 3679−86.
31. Wang C, Lee MR. High-level expression of soluble rat hsc70 in *Escherichia coli*: purification and characterization of the cloned enzyme. *Biochem J* 1993;**294**:69−77.
32. Wang TF, Chang JH, Wang C. Identification of the peptide binding domain of hsc70. 18-kilodalton fragment located immediately after ATPase domain is sufficient for high affinity binding. *J Biol Chem* 1993;**268**:26049−51.
33. Terlecky SR, Chiang HL, Olson TS, Dice JF. Protein and peptide binding and stimulation of *in vitro* lysosomal proteolysis by the 73-kDa heat shock cognate protein. *J Biol Chem* 1992;**267**:9202−9.
34. Chen D, Cai J, Yin J, Jiang J, Jing C, Zhu Y, et al. Lycorine-derived phenanthridine downregulators of host Hsc70 as potential hepatitis C virus inhibitors. *Future Med Chem* 2015;**7**:561−70.
35. Chen DZ, Fan SR, Yang BJ, Yao HC, Wang YT, Cai JY, et al. Phenanthridine derivative host heat shock cognate 70 down-regulators as porcine epidemic diarrhea virus inhibitors. *J Nat Prod* 2021;**84**: 1175−84.
36. Ktistakis NT, Tooze SA. Digesting the expanding mechanisms of autophagy. *Trends Cell Biol* 2016;**26**:624−35.
37. Bjorkoy G, Lamark T, Brech A, Outzen H, Perander M, Overvatn A, et al. p62/SQSTM1 forms protein aggregates degraded by autophagy and has a protective effect on huntingtin-induced cell death. *J Cell Biol* 2005;**171**:603−14.
38. Xie Z, Klionsky DJ. Autophagosome formation: core machinery and adaptations. *Nat Cell Biol* 2007;**9**:1102−9.
39. Aniento F, Roche E, Cuervo AM, Knecht E. Uptake and degradation of glyceraldehyde-3-phosphate dehydrogenase by rat liver lysosomes. *J Biol Chem* 1993;**268**:10463−70.
40. Yang Q, Mao Z. The complexity in regulation of MEF2D by chaperone-mediated autophagy. *Autophagy* 2009;**5**:1073−4.
41. Wang S, Yin J, Chen D, Nie F, Song X, Fei C, et al. Small-molecule modulation of Wnt signaling *via* modulating the Axin-LRP5/6 interaction. *Nat Chem Biol* 2013;**9**:579−85.
42. Zheng M, Feng B, Zhang Y, Liu X, Zhao N, Liu H, et al. Discovery and characterization of novel potent non-covalent small molecule inhibitors targeting papain-like protease from SARS-CoV-2. *Acta Pharm Sin B* 2024;**14**:3286−90.
43. Lo HS, Hui KPY, Lai HM, He X, Khan KS, Kaur S, et al. Simeprevir potently suppresses SARS-CoV-2 replication and synergizes with remdesivir. *ACS Cent Sci* 2021;**7**:792−802.
44. Fan L, Zhou Y, Wei X, Feng W, Guo H, Li Y, et al. The E3 ligase TRIM22 restricts SARS-CoV-2 replication by promoting proteasomal degradation of NSP8. *mBio* 2024;**15**:e0232023.
45. Rudiger S, Germeroth L, Schneider-Mergener J, Bukau B. Substrate specificity of the DnaK chaperone determined by screening cellulose-bound peptide libraries. *EMBO J* 1997;**16**:1501−7.
46. Mayer MP. Hsp70 chaperone dynamics and molecular mechanism. *Trends Biochem Sci* 2013;**38**:507−14.
47. Hartl FU, Hayer-Hartl M. Molecular chaperones in the cytosol: from nascent chain to folded protein. *Science* 2002;**295**:1852−8.
48. Wu L, Zhang L, Feng S, Chen L, Lin C, Wang G, et al. An evolutionarily conserved ubiquitin ligase drives infection and transmission of flaviviruses. *Proc Natl Acad Sci U S A* 2024;**121**:e2317978121.
49. Snijder EJ, Limpens R, de Wilde AH, de Jong AWM, Zevenhoven-Dobbe JC, Maier HJ, et al. A unifying structural and functional model of the coronavirus replication organelle: tracking down RNA synthesis. *PLoS Biol* 2020;**18**:e3000715.
50. Xu S, Wang Y, Shi D, Wang S, Qiao L, Yang G, et al. Discovery and mechanism verification of first-in-class hydrophobic tagging-based degraders of HBV core protein. *Acta Pharm Sin B* 2025;**15**:2170−96.
51. Wei X, Zhou Y, Shen X, Fan L, Liu D, Gao X, et al. Ciclopirox inhibits SARS-CoV-2 replication by promoting the degradation of the nucleocapsid protein. *Acta Pharm Sin B* 2024;**14**:2505−19.
52. Rosenzweig R, Sekhar A, Nagesh J, Kay LE. Promiscuous binding by Hsp70 results in conformational heterogeneity and fuzzy chaperone-substrate ensembles. *eLife* 2017;**6**:e28030.
53. Tian L, Qiang T, Liang C, Ren X, Jia M, Zhang J, et al. RNA-dependent RNA polymerase (RdRp) inhibitors: the current landscape and repurposing for the COVID-19 pandemic. *Eur J Med Chem* 2021; **213**:113201.